Three-dimensional computer simulations of local and line-of-sight integrated H_α line emission in the TEXTOR helical divertor

H. Frerichs[1], D. Reiter[1], M. Clever[1], Y. Feng[2]

[1] *Institute for Energy Research - Plasma Physics, Forschungszentrum Jülich GmbH, Germany*

[2] *Max-Planck-Institut für Plasmaphysik, Greifswald, Germany*

Introduction

The recent interest in resonant magnetic perturbations (RMPs) applied at the plasma edge of several tokamak experiments demands for 3D transport simulations to interpret experimental observations. One such simulation tool is the EMC3-EIRENE code [1, 2], which we apply to the helical divertor configuration at the TEXTOR tokamak [3]. This configuration is characterized by a very complex magnetic field structure at the plasma edge: flux tubes of short connection length are embedded in domains of chaotic field line behavior with long connection length. Divertor properties of such a configuration can be analyzed experimentally by the Balmer series emission (e.g. H_α at $\lambda = 656\,\mathrm{nm}$) observed by CCD cameras, but deconvolution to obtain local information is demanding, in particular in 3D configurations. We therefore analyze the relation between local and line-of-sight integrated H_α emission, using computer simulations.

Data post-processing in hexahedral grids

The H_α-light in the TEXTOR helical divertor is calculated on the basis of 3D edge plasma simulations with the EMC3-EIRENE code. Characteristic parameters - such as electron density n_e, electron temperature T_e and neutral hydrogen density n_H - are provided by the code within each cell of a 3D hexahedral grid. This grid is divided into several, magnetic field aligned blocks (see fig. 1), which allows a fast reconstruction of magnetic field lines [4]. The iso-parametric concept (which is well-known in finite element methods) introduces so called natural coordinates $\boldsymbol{\xi} = (\xi, \eta, \zeta)$, which are related to real space (here cylindrical) coordinates $\mathbf{R} = (R, Z, \varphi)$ by

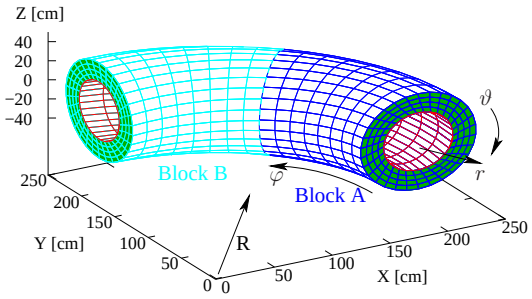

Figure 1: Magnetic field aligned grid with two toroidal blocks.

$$\mathbf{R}(\boldsymbol{\xi}) = \sum_{a=1}^{8} N_a(\boldsymbol{\xi})\, \mathbf{R}_a. \tag{1}$$

N_a are shape functions of a trilinear hexahedron (see [5] for more details) and $\mathbf{R}_a$ are the coordinates of the 8 nodes. While magnetic field lines are reconstructed from coordinate lines

ζ = const, the iso-parametric concept is general enough to allow interpolation of any quantity F defined on grid nodes:

$$F(\boldsymbol{\xi}) \;=\; \sum_{a=1}^{8} N_a(\boldsymbol{\xi})\, F_a, \tag{2}$$

by using the inverse of (1) to obtain the natural coordinates $\boldsymbol{\xi}$ corresponding to a given point $\mathbf{R}$. However, for (2) to be applicable to data provided by the EMC3-EIRENE code, it is necessary to provide a mapping `cell2node` of cell averaged data $\mathbf{f} \in \mathbb{R}^{n_{\text{cells}}}$ to the surrounding grid nodes. Each node value F_j is defined by the weighted average

$$\texttt{cell2node} : \mathbb{R}^{n_{\text{cells}}} \to \mathbb{R}^{n_{\text{nodes}}}, F_j \;=\; \frac{1}{W_j} \sum_{i \in C_j} w_i\, f_i, \qquad W_j \;=\; \sum_{i \in C_j} w_i, \tag{3}$$

where C_j is the set of cells that are connected to node j and $w_i = 1/V_i$ is the weight for each cell given by its volume (see [5] for details regarding block boundaries). Now (2) can be used for data arrays provided by the EMC3-EIRENE code, but also for derived data such as the emitted H_α light. Both the EIRENE code database AMJUEL and the ADAS project [6] e.g. provide photon emissivitiy coefficients $\mathcal{P} = \mathcal{P}(n_e, T_e)$ for specific lines, which can be used to obtain the local radiated energy P_{H_α} (i. e. $\Delta E \cdot$ H_α emissivity):

$$P_{H_\alpha} \;=\; n_e \cdot n_H \cdot \Delta E \cdot \mathcal{P}(n_e, T_e), \qquad \Delta E \;=\; \frac{h\,c}{\lambda} \tag{4}$$

The setup of the camera system at TEXTOR is sketched in fig. 2, showing a tangential view on the divertor target at $\varphi_{\text{cam}} = 154.7$ deg. In order to compare the local H_α emission to a simulated camera image, we introduce a 2D reference grid in the $r-\vartheta$ plane (i.e. observation plane in fig. 2). The local value of P_{H_α} is evaluated at each grid point $\mathbf{x}$ (in Cartesian coordinates), while the corresponding line-of-sight integrated value (camera pixel) is obtained by the discretization of resolution $2L+1$:

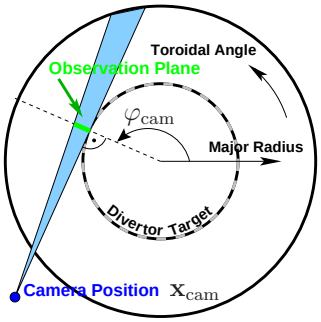

Figure 2: Setup of the camera system at TEXTOR.

$$\mathfrak{P}_{H_\alpha} \;=\; \sum_{k=0}^{2L} \Delta l\, P_{H_\alpha}(\mathbf{l}_k), \qquad \mathbf{l}_k \;=\; \mathbf{x}_{\text{cam}} + \frac{k}{L}(\mathbf{x} - \mathbf{x}_{\text{cam}}), \qquad \Delta l \;=\; \frac{1}{L}\,|\mathbf{x} - \mathbf{x}_{\text{cam}}|\,. \tag{5}$$

Analysis of local and line-of-sight integrated H_α emission

We now apply this procedure to a TEXTOR helical divertor scenario, for which the local wall-to-wall connection length l_c of magnetic field lines in front of the DED target at φ_{cam} is shown in fig. 3 (a). The local P_{H_α} distribution obtained from 3D edge transport simulations with the

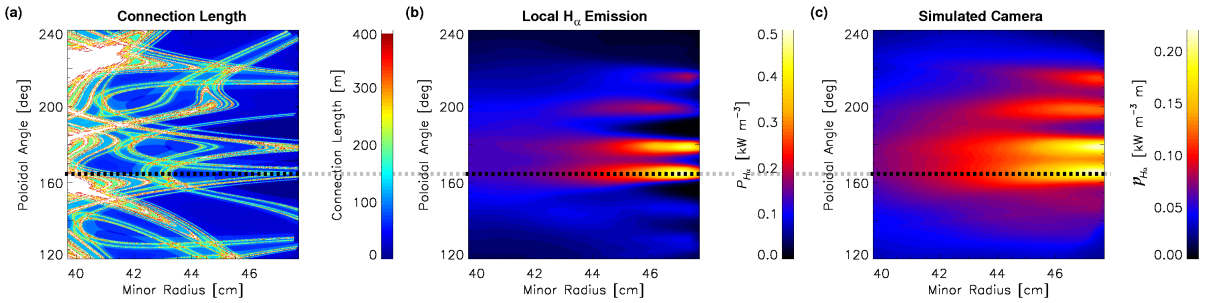

Figure 3: 2D cuts at φ_{cam}: (a) Connection length of field lines and (b) local H_α emission. (c) Simulated camera image (i.e. line-of-sight integrated values).

boundary condition $n_{\text{in}} = 1.0 \cdot 10^{19}\,\text{m}^{-3}$ at the inner simulation boundary (red surface in fig. 1) is shown in fig. 3 (b). The corresponding (simulated) camera image is given in fig. 3 (c). Radial profiles at $\vartheta = 165$ deg are extracted in fig. 4 for better comparison (red lines). Furthermore, profiles from simulations with higher n_{in} are shown as well. The peaks of $\mathfrak{P}_{H_\alpha}$ are located in all cases approx. 5 mm closer to the target plates at $r_{\text{target}} = 47.7\,\text{cm}$ than the peaks of P_{H_α}, which is demonstrated in fig. 5 (red lines). This shift is related to the non-local character of the line-of-sight integration. As can be seen in fig. 6 (a), there are contributions to $\mathfrak{P}_{H_\alpha}$ over more than $\Delta L = 40\,\text{cm}$ (i.e. $\Delta\varphi \approx 20$ deg) along the line-of-sight and the largest contribution is not necessarily located at the observation plane.

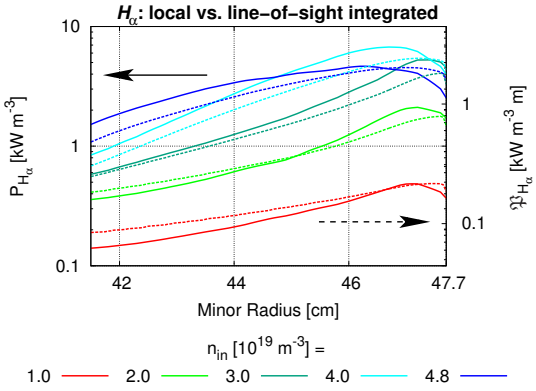

Figure 4: Radial profiles of P_{H_α} (solid) and $\mathfrak{P}_{H_\alpha}$ (dashed) at $\vartheta = 165$ deg at different densities.

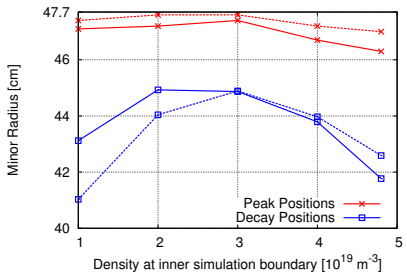

Figure 5: Peak and decay positions of the P_{H_α} (solid) and $\mathfrak{P}_{H_\alpha}$ (dashed) profiles from fig. 4.

The blue profiles in fig. 5 mark the decay positions, i.e. where the radial profiles in fig. 4 have fallen to $1/e$ of their respective peak values. It can be seen that the penetration depth of H_α light, as estimated by the simulated camera, is overestimated by $\sim 2\,\text{cm}$ for low n_{in} and underestimated by $\sim 1\,\text{cm}$ for high n_{in}. However, the general features of both profiles are the same: At first, the decay positions move towards the target with increasing density. This is caused by a decrease of the penetration depth for neutral particles, related to an increasing ionization (and scattering) rate S_p in front of the target (see fig. 6 (c)). At even higher densities, the temperature drops to a significant low level (below 5 eV near the

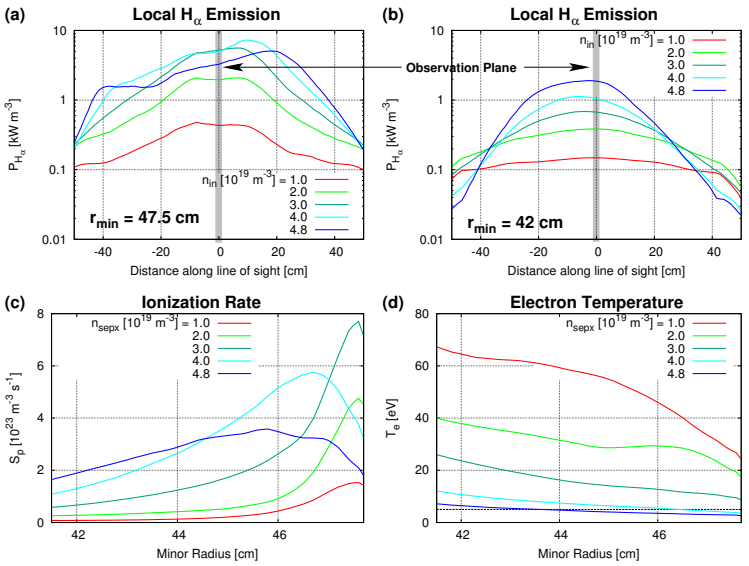

Figure 6: Line-of-sight profiles of P_{H_α} for a reference position of $\vartheta = 165$ deg and $r = 47.5\,\mathrm{cm}$ (a) and $r = 42\,\mathrm{cm}$ (b). Radial profiles of S_p (c) and T_e (d).

target, see fig. 6 (d)), resulting in a net decrease of the ionization rate, and hence, a deeper penetration of neutral particles combined with a reduction of H_α emission near the target. The reason for the difference between the P_{H_α} and $\mathfrak{P}_{H_\alpha}$ decay position at low and high n_{in} can be found in fig. 6 (b) in comparison to (a). Line-of-sight profiles for the reference point $r = 42\,\mathrm{cm}$ show that for low n_{in} there are contributions to $\mathfrak{P}_{H_\alpha}$ over a larger distance ΔL than for high n_{in}. This is significantly different at the reference point $r = 47.5\,\mathrm{cm}$ and results in the alleged deeper penetration at low n_{in}.

Conclusions

The iso-parametric concept allows to interpolate and integrate 3D plasma data (obtained with EMC3-EIRENE) at any given point within a computational grid, when cell averaged data provided by transport simulations is mapped to the grid nodes. This procedure allows to generate virtual camera images of H_α emission by line-of-sight integration, i.e. by sending one ray per camera pixel. Comparisons to the local H_α emission have shown significant differences in the detailed structure, such as the peak and decay positions, but also similarities in the general behavior during a density scan. A comparison to experimental observations and an analysis of line-of-sights perpendicular to the target (at $\varphi \approx 200$ deg) are left for future studies.

References

[1] Y. Feng et al., *Contrib. Plasma Phys.* **44**, 1-3, 57 (2004)

[2] D. Reiter et al., *Fusion Science and Technology* **47**, 172 (2005)

[3] O. Schmitz et al., *Nuclear Fusion* **48** (2008) 024009

[4] Y. Feng et al., *Physics of Plasmas* **12**, 052505 (2005)

[5] H. Frerichs, "Three-dimensional plasma transport in open chaotic magnetic fields: A computational assessment for tokamak edge layers" *Berichte des Forschungszentrum Juelich* (2010) Juel-4321, ISSN: 0944-2952

[6] H. P. Summers et al., *Plasma Phys. Control. Fusion* **48** (2006) 263-293